Izraylit, V.; Gould, O.; Kratz, K.; Lendlein, A.:
Investigating the Phase-Morphology of PLLA-PCL Multiblock Copolymer / PDLA Blends Cross-linked Using Stereocomplexation.
In: MRS Advances. Vol. 5 (2020) 14 – 15, 699 - 707.
First published online by Cambridge University Press: 16.12.2019

https://dx.doi.org/10.1557/adv.2019.465

Investigating the Phase-Morphology of PLLA-PCL Multiblock Copolymer / PDLA Blends Cross-linked Using Stereocomplexation

Victor Izraylit[1,2], Oliver E. C. Gould[1], Karl Kratz[1], Andreas Lendlein[1,2*]

[1] *Institute of Biomaterial Science and Berlin-Brandenburg Centre for Regenerative Therapies, Helmholtz-Zentrum Geesthacht, Kantstrasse 55, 14513 Teltow, Germany*
[2] *Institute of Chemistry, University of Potsdam, Karl-Liebknecht-Str. 24/25, 14476 Potsdam, Germany*

ABSTRACT

The macroscale function of multicomponent polymeric materials is dependent on their phase-morphology. Here, we investigate the morphological structure of a multiblock copolymer consisting of poly(L-lactide) and poly(ε-caprolactone) segments (PLLA-PCL), physically cross-linked by stereocomplexation with a low molecular weight poly(D-lactide) oligomer (PDLA). The effects of blend composition and PLLA-PCL molecular structure on the morphology are elucidated by AFM, TEM and SAXS. We identify the formation of a lattice pattern, composed of PLA domains within a PCL matrix, with an average domain spacing d0 = 12 – 19 nm. The size of the PLA domains were found to be proportional to the block length of the PCL segment of the copolymer and inversely proportional to the PDLA content of the blend. Changing the PLLA-PCL / PDLA ratio caused a shift in the melt transition Tm attributed to the PLA stereocomplex crystallites, indicating partial amorphous phase dilution of the PLA and PCL components within the semicrystalline material. By elucidating the phase structure and thermal character of multifunctional PLLA-PCL / PDLA blends, we illustrate how composition affects the internal structure and thermal properties of multicomponent polymeric materials. This study should facilitate the more effective incorporation of a variety of polymeric structural units capable of stimuli responsive phase transitions, where an understanding the phase-morphology of each component will enable the production of multifunctional soft-actuators with enhanced performance.

INTRODUCTION

Biodegradable polymers such as polylactones [1] and their blends are highly desirable for the creation of degradable implants [2, 3], drug delivery systems [4, 5] and sustainable packaging solutions [6]. The synthetic alteration of lactide-based copolyesters and their combination with other polymeric segments has led to the

determination of a structure-property relationship and enabled tailoring of their bulk properties [7, 8], with the realization of emergent behavior unseen in homopolymer materials [9-11]. However, the combination of multiple chemically distinct entities (e.g. segments in block copolymers or blend components) must overcome issues with their compatibility to control the resulting matrix architecture and subsequent function [12, 13]. It is essential to understand the distribution of each polymeric component within the material.

Polylactide (PLA) is a bioresorbable thermoplastic material, whose potential applications have been limited by its high stiffness and inherent brittleness (E = 1.5 – 4 GPa, ε_{break} < 100% in ambient conditions) [14]. Poly(ε-caprolactone) (PCL) is a highly elastic biodegradable polymer, with significantly higher mechanical stability (E = 0.2 – 0.4 GPa, ε_{break} up to 1000% in ambient conditions) [15]. The combination of these two polymers gives a semicrystalline material with two thermally distinct crystalline domains, from PCL ($T_g \approx$ –60 °C and $T_m \approx$ 60 °C) [14] and PLA ($T_g \approx$ 60 °C and $T_m \approx$ 170 °C)[15], and greatly enhanced mechanical properties.

Blending approaches provide a low-cost and efficient means to combine the two polymers, where the blend ratio can be used to tune the thermal and mechanical properties of the materials [16]. However, due to their immiscibility [17], phase separation leads to inhomogeneity within the material [18]. The blending of PLA and PCL homopolymers has been demonstrated to result in the formation of micrometer-scale droplets of the minority component with sizes dependent on the blend ratio [19]. Altering the PCL-to-PLA ratio within the blend also resulted in an approx. 10 °C change in the measured melting temperature of PCL, caused by a variation in the interpenetration of PCL and PLA amorphous phases within the semicrystalline material.

The synthetic realization of copolymers with both PCL and PLA segments has enabled the creation of materials with higher phase interpenetration than their homopolymer blend equivalents. Bi-continuous lamellar or cylindrical morphologies are formed dependant on the ratio of two segments within the material [20]. Within the semicrystalline material the separated amorphous domains of the PLA and PCL copolymer segments can partially interpenetrate, resulting in a composition-dependent shift of the maximum in the PLA melting transition of up to 15 °C [21, 22].

Crystallization plays an important role in determining the morphological structure of the material. Upon cooling, the crystallization of PLA and PCL domains drives further phase separation, observed by SAXS, before an increase in miscibility is observed upon melting [20]. The introduction of PLA stereocomplexation has recently received interest for the creation of tuneable physical netpoints within pseudo-cross-linked matrices [23]. The corresponding increase in PLA crystallization rate, caused by the energetic favourability of stereocomplex crystallites [24], has been shown to promote phase separation in PLA-based copolymer blends [25, 26]. Further clarification of the roles of these different compositional elements, specifically their spatial distribution and structure, should enhance our control over the thermal and mechanical characteristics of multicomponent polymeric materials.

In this work we investigate the phase-morphology of a blend material, consisting of a multiblock copolymer with poly(*L*-lactide) and poly(ε-caprolactone) segments (PLLA-PCL) and a poly(*D*-lactide) oligomer (PDLA). Within this material, PDLA molecules and PLLA segments form a physically crosslinked network via PLA stereocomplexation. Through investigation with SAXS, AFM, TEM and DSC we elucidate the phase-morphology of PLLA-PCL / PDLA blends and its influence on the thermal properties of the material.

EXPERIMENTAL SECTION

Material preparation

The multiblock copolymer containing poly(*L*-lactide) and poly(ε-caprolactone) segments was synthesized as reported elsewhere [27, 28].

Three batches of PLLA-PCL were synthesized in this work: PLLA12-PCL58, PLLA15-PCL64 and PLLA12-PCL20, where numbers stand for number average lengths of the respective segments as determined with ^{1}H NMR. The weight average molecular weight M_w of all of the PLLA-PCL batches were similar around 500 kg · mol^{-1} determined by a multidetector GPC setup. The difference in molecular characteristics between the two batches (PLLA12-PCL58 and PLLA15-PCL64) were found to be insignificant within margin of error of the used techniques (12% and 10% of the measured value for ^{1}H NMR and GPC respectively).

Poly(*D*-lactide) (PDLA) was synthesized via the ring-opening polymerization of *D*,*D*-dilactide (99.5%, Corbion, Amsterdam, Netherlands), using tin(II)-*2*-hexanoate ($Sn(Oct)_2$) (96%, Alfa Aesar, Ward Hill, USA) as the catalyst and 1-hexanol (99%, Acros Organics, Geel, Belgium) as the initiator. The number average molecular weight of PDLA was determined with ^{1}H NMR as M_n = 1.9 kg · mol^{-1}.

Films were prepared via solution casting. The polymers were dissolved at a predetermined ratio in chloroform (99.9%, Carl Roth, Karlsruhe, Germany). The solution was stirred for 3 hours until the polymers were dissolved, before pouring into a polytetrafluoroethylene (PTFE) Petri dish, covering with aluminium foil and left to evaporate in ambient conditions for 2 days. The produced blends were named as PLLA12-PCL58-SCX, were X stays for the weight content of PDLA in the blends.

Nuclear magnetic resonance spectroscopy (NMR)

^{1}H NMR spectra were recorded using a DRX Avance 500 MHz spectrometer (Bruker, Rheinstetten, Germany) at room temperature in deuterated chloroform. Chemical shifts (δ) are reported in parts per million (ppm) relative to residual chloroform at δ 7.26 ppm. Samples were dissolved in $CDCl_3$ at concentration of 15 mg·mL^{-1}. The spectra were evaluated according to the position and intensity of signals as reporter elsewhere.[29]

X-ray crystallographic analysis

Weight average molecular weights of starting materials and products were determined by gel permeation chromatography (GPC), using a Tosoh EcoSEC HLC-8320 Gel Permeation Chromatograph equipped with a refractive index detector (Tosoh Bioscience, Stuttgart, Germany) combined with a PSS Universal Data Center (PSS, Mainz, Germany), a viscometer ETA2010 (PSS, Mainz, Germany), an EcoSEC UV detector 8320 (Tosoh Bioscience), a light scattering detector SLD7100 (PSS, Mainz, Germany) and two HT-GPC columns type PSS SDV analytical linear M 5 µm (PSS, Mainz, Germany) connected in series. For the measurements, by universal calibration, tetrahydrofuran (THF) was used as an eluent (35 °C, 1.0 mL·min^{-1}) with 0.05 weight content 3,5-di-*tert*-butyl-4-hydroxytoluene as an internal standard. Molecular weight calculations were performed using WINGPC 6.2 (PSS) SEC software (Polymer Standard Service, Mainz, Germany).

Differential scanning calorimetry (DSC)

DSC experiments were conducted on a Netzsch DSC 204 Phoenix (Selb, Germany) at heating and cooling rates of 10 °C·min^{-1} in pierced aluminum pans. For determining the thermal properties of the polymers and blends, the materials were scanned in the temperature range -100 – 200 °C. The crystallinity of all components was calculated according to the equation:

$$\chi_c = \frac{\Delta H_m}{\Delta H_m^{100} \cdot W} \cdot 100$$

Where ΔH_m is the experimental melting enthalpy of a fraction, determined as the area under the melting peak. ΔH_m^{100} is the specific melting enthalpy of 100% crystalline polymer, which is 135 J·g^{-1} for PCL [30] and 142 J·g^{-1} for PLA stereocomplex [31]. *W* is the weight content of the fraction in the copolymer of the blend. The PLA stereocomplex fraction was calculated as the maximal amount of coupling *L*- and *D*-lactide units. The data was registered at the first cooling and the second heating run.

X-ray crystallographic analysis

Wide angle X-ray scattering (WAXS) measurements were performed with a D8 Discover spectrometer with a 2D-detector from (Bruker AXS, Karlsruhe, Germany) in the temperature range 25 – 70 °C. The samples of dimensions 2 x 0.5 cm and width 150 µm were fixed at both ends during characterization.

Small angle X-ray scattering (SAXS) experiments were performed on a Bruker Nanostar diffractometer (Bruker AXS, Karlsruhe, Germany), using a 400 µm beam with a wavelength of 0.15418 nm (CuKα) and a Vantec-2000 detector (2048*2048 pixel, 68 µm pixel size) to record scattered intensities at a distance of 1050 mm from the samples.

Transition electron microscopy (TEM)

TEM investigations were performed on a Talos F200A (FEI, Eindhoven, The Netherlands) with high-brightness electron source (X-FEG) and an information limit of 0.12 nm. The prepared samples were all analyzed at 200 kV using a CompuStage Single-Tilt holder (FEI, Eindhoven, The Netherlands). The images were obtained with a CMOS technology based camera model Ceta 16M (FEI, Eindhoven, The Netherlands) with a resolution of 4000×4000 pixels. The samples were prepared by cutting with a diamond knife. The cuts were deposited at Lacey-carbon film on 400 mesh copper grid with 42 µm mesh size. The surface area morphology was evaluated using ImageJ software.

Atomic force microscopy (AFM)

AFM measurements were performed by AFM Multimode with NanoScope V Controller with Veeco thermal application controller (Veeco Instrument Inc., New York, USA). The samples were prepared by cutting with a diamond knife. Samples with an approximate thickness of 100 nm were then placed on a silica grid, before scanning at ambient temperature (25 °C). Imaging was performed in a tapping mode with a scan rate of 0.8–1.0 Hz. An RTESPA-150 probe (Bruker, Karlsruhe, Germany) with a typical driving frequency of 150 kHz (individual difference ranged from 90 to 210 kHz) and a typical spring constant of 5 N·m^{-1} (individual difference ranged from 1.5 to 10 N·m^{-1}) was used. The tip radius and height were 10 – 15 nm and 10 ± 2 µm respectively. The tip

was of rectangular shape with a front angle of 15 ±2 °, a side angle of 17.5 ±2 ° and a back angle of 25 ± 2°. Scans sizes of 1 ×1 μm were chosen to visualize the morphology of the material.

Dynamic mechanical thermal analysis (DMTA)

DMTA measurements were performed using an Eplexor 25 N (Gabo, Ahlden, Germany) equipped with a 25 N load cell using a standard test specimen type (DIN EN ISO 527-2/1BB). The applied oscillation frequency was 1 Hz. The measurement was performed in the temperature sweep mode from −100 to 100 °C with a constant heating rate of 1 °C·min−1. The glass transition (T_g) was determined at the peak maximum of loss modulus (E'') vs temperature curve.

RESULTS AND DISCUSSION

Thermal properties

The thermal characteristics of the samples, obtained from differential scanning calorimetry (DSC) analysis, are shown in Table I. Glass transition T_g was not visible in DSC. Mixed glass transition T_g = – 40 ± 3 °C was determined for all studied samples as maximum of loss modulus E'' in dynamic mechanical thermo-analysis (DMTA). A mixed glass transition indicates interpenetration of PLA and PCL amorphous phases [32]. A thermal transition of PLLA12-PCL58 attributed to the melting of PCL domains within the material was observed with a peak maximum at T_m = 52 ± 1 °C with a melting enthalpy ΔH corresponding to a relative crystallinity χ_c = 36 ± 4%. PLA homopolymer is incapable of crystallization at block lengths of lower than 7 repeating units [33]. PLA stereocomplex, being an energetically preferable structure, can be formed with only 5 repeating units. However, the additional loss of flexibility of the chain as a result of its incorporation in a multiblock copolymer structure, renders several end monomer units of each block unavailable for crystallization. The minimal block length required for crystallization and stereocomplexation of PLLA segments within a multiblock copolymer is slightly higher. 12 – 15 repeating units were experimentally determined for the polymer samples presented here to be sufficient for PLA stereocomplex formation, but still too short for the formation of pure PLLA crystallites. This is supported by the absence of a PLLA melting transition in DSC. The observed melt transition of PCL T_m remains similar with the addition of up to 10 wt.% PDLA into the blend. PCL crystallinity was observed to increase to χ_c = 48 ± 5% in PLLA12-PCL58-SC2 and further decrease to χ_c = 38 ± 4% with the increase of PDLA content to 10 wt.%. Block copolymer segments generally hinder the crystallization of each other, however, segments of close compositions have been reported to support crystallization of neighboring units [34, 35]. The cross-link density, i.e. the PLA stereocomplex content, did not appear to disturb the crystallinity of the PCL matrix, while the introduction of cross-links formed from covalent chemical bonding generally disrupt the ability of a material to crystallize [36]. DSC traces of all of the blend samples possess a broad PLA stereocomplex melting transition with a maximum in the region of T_m = 171 – 181 °C. The observed lower melt transition T_m, when compared to that reported in the literature T_m > 200 °C, is the result of the low M_w of the PLLA segment [24] and dilution of the amorphous phases of PLA and PCL [19, 21, 22]. The increase in T_m of PLA stereocomplex and absence of any effect on T_m of PCL with the increase of PDLA content in the matrix suggests that although PLLA and PCL amorphous phases of the

pure PLLA-PCL are partially interpenetrated, PDLA has higher affinity to the PLLA part of the matrix and does not dilute the PCL amorphous phase. A decrease in the crystallinity of the PLA stereocomplex from χ_c = 57 ± 6% to 35 ± 4% was observed, with higher values in the blends with higher PDLA content.

Table I. Thermal properties of PLLA-PCL and its PDLA blends obtained from DSC

Sample[a]	**PCL***			**PLA stereocomplex***		
	ΔH $(J \cdot g^{-1})^b$	T_m (°C)[b]	χ_c (%)[c]	ΔH $(J \cdot g^{-1})^b$	T_m (°C)[b]	χ_c (%)[c]
PLLA12-PCL58	42±4	52±1	36±4	-	-	-
PLLA12-PCL58-SC1	42±4	54±1	42±5	1.6±0.2	177±1	57±6
PLLA12-PCL58-SC2	43±5	54±1	44±5	2.3±0.2	181±1	41±4
PLLA12-PCL58-SC5	42±4	54±1	46±5	5±0.5	180±1	35±4
PLLA12-PCL58-SC10	34±3	42±1	38±4	10±1	171±1	37±4

* Attributed to the respective crystalline domains according to literature data. [a] Sample name PLLAX-PCLY-SCZ where X and Y stay for number average block length of PLLA and PCL respectively in PLLA-PCL multiblock copolymer respectively, determined with ^{1}H NMR, Z stays for PLLA-PCL / PDLA wt. ratio of the blend. [b] Intrinsic melting enthalpy, as the peak area, and melting temperature, as the peak maximum position. [c] Degree of crystallinity, as the ratio between ΔH and $\Delta\Delta_\Delta^{\Delta\Delta\Delta}$ of 100% crystalline polymers. T_g was not visible in DSC measurements and was determined as T_g = –40 ± 3 °C for all samples with DMTA. DSC error was considered according to technical specification of the equipment.

Crystalline structure

The crystalline structure of the materials was studied by WAXS at room temperature. A representative WAXS profile is presented in Figure 1. The PCL crystalline reflections (110) and (200) in the positions 2θ = 21.5° and θ = 24° respectively overlap with PLA stereocomplex (300) and (030) signals at 2θ = 20.5° an (220) at 2θ = 24°. A singular 2θ = 12° signal originates from the scattering of the (110) PLA stereocomplex plane. The absence of a significant signal in 2θ = 16° region further confirms the incapability of PLLA segments or PDLA molecules to crystallize outside of stereocomplexation. The presence of PCL crystallites in the pure multiblock copolymer samples PLLA12-PCL58 and PLLA12-PCL20 was observed. Both PCL crystalline domains and PLA stereocomplexes crystallites were observed in the structure of the blends PLLA12-PCL58-SC10 and PLLA12-PCL20-SC20.

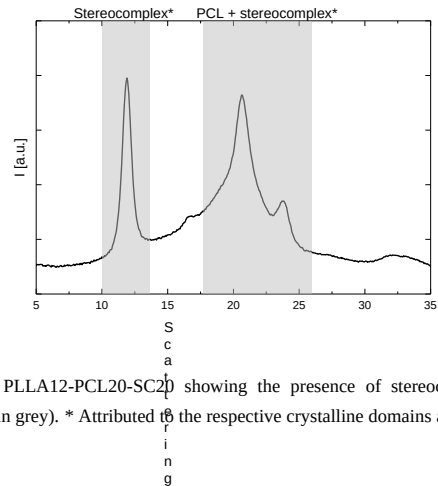

Figure 1. WAXS spectra of PLLA12-PCL20-SC20 showing the presence of stereocomplex crystallites and PCL crystalline domains (indicated in grey). * Attributed to the respective crystalline domains according to the literature data.

Phase-morphology

To understand the phase-morphology of the material depending on its composition and the distribution of PCL and PLA domains, AFM, TEM and SAXS were used to characterize the samples.

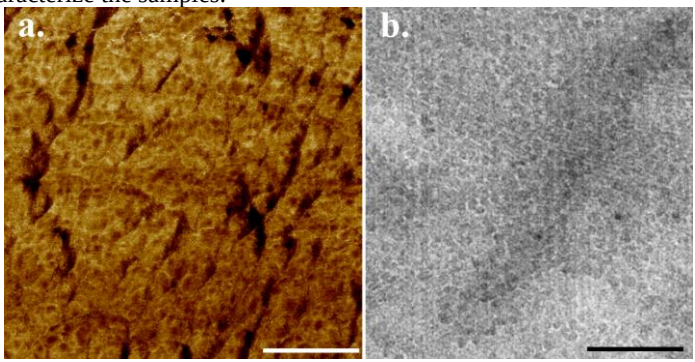

Figure 2. (a) AFM phase image and (b) TEM image of PLLA15-PCL64-SC1. Scale bar 200 nm.

AFM phase imaging at 25 °C (Figure 2a) shows distinct separation between harder and softer domains. Softer regions with a diameter of d = 18 – 25 nm are surrounded by harder regions with width h = 4 – 8 nm. As imaging was performed at a temperature higher than the T_g of PLA, as measured by DMTA, we attribute the softer areas to the PLA domains that exist in an amorphous state in this sample (Table I). The higher crystallinity of the PCL within the material should cause higher local mechanical stiffness, resulting in a contrast difference between the two components by AFM phase imaging. We therefore attribute the harder regions to crystalline PCL.

TEM images taken at 25 °C, as shown in Figure 2b, reveal a similar microphase separated lattice morphology. The average domain spacing d = 10 – 20 nm is in agreement with the AFM findings. The displayed images are representative of all of the studied blend samples and a similar morphology was also observed for the pure PLLA-PCL sample. The form of the domains did not change with the variation of PLLA-PCL block structure, PLLA-PCL / PDLA blend ratio and crystallinity of the components of the matrix. The similarity in the morphology observed by TEM, where differences in electron density provide contrast, and AFM phase imaging, where differences in mechanical stiffness provide contrast, indicates that the observed domains are chemically and mechanically distinct. Based on the observed difference in electron density and local mechanical stiffness of the islands and the spaces between them, we believe that the islands are formed of predominantly amorphous PLA and contain the PLA stereocomplex crystallites, while the spacing is formed of predominantly crystalline PCL. Additional PCL crystalline lamellae can also be seen in the TEM images.

The observed change in the maximum of the melt transition attributed to the PLA stereocomplex, as measured by DSC, provides evidence of PLA/PCL amorphous phase dilution. As the PLA content of the material is increased the relative disruption of PLA crystallization by amorphous PCL segments is reduced, leading to an increase in melting temperature. Despite the partial interpenetration of the amorphous phase of both polymer segments, they remain phase separated.

SAXS analysis was performed to further characterize the observed morphological features. The average domain spacing was calculated as a maximum of

the $I(d)\cdot q^2$ function (Figure 3a). The results further support the AFM and TEM data, with a strong maximum measured corresponding to d_0 = 15 – 20 nm, which we attribute to the morphological domain observed by TEM and AFM. The observed second maximum in the $2q_0$ region for all of the curves implies presence of ordered structures. A linear dependency of d_0 on the matrix composition was observed for the PLLA15-PCL64-SCX blends in the studied region (Figure 3b). However, the pure multiblock copolymer PLLA15-PCL64 did not follow this trend, indicating that stereocomplexation affects the microphase separation. An increase in the PDLA content of the material, and subsequently the PLA stereocomplex content reduces d_0 as a result of the denser packing of PLA domains with the increase in crystallization. The shorter PCL average segment length of PLLA12-PCL20, results in a lower value of d_0 = 15.8 nm, which further decreases to a value of 12.1 nm in the PLLA12-PCL20-SC20 blend.

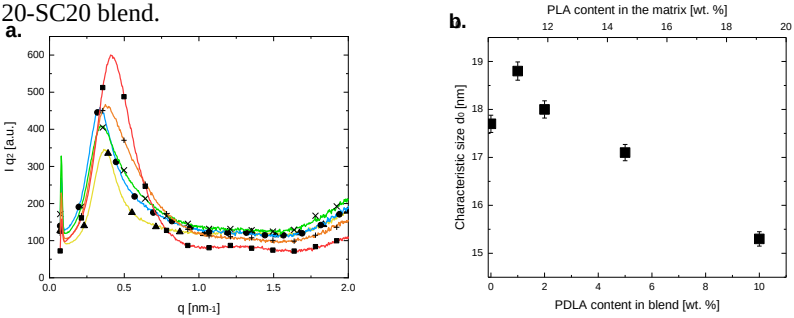

Figure 3. (a) SAXS spectra of PLLA15-SC64 – yellow (triangles), PLLA15-SC64-SC1 – blue (circles), PLLA15-SC64-SC2 – green (cross symbol), PLLA15-SC64-SC5 – orange (plus symbol) and PLLA15-SC64-SC10 – red (squares). (b) Effect of PDLA content in PLLA15-SC64 blends on the average domain spacing studied by SAXS.

CONCLUSION

In this work we investigate the morphology of blends composed of a multiblock copolymer (PLLA-PCL) containing poly(*L*-lactide) and poly(ε-caprolactone) segments and a poly(*D*-lactide) oligomer (PDLA). Different PLLA-PCL block structures (20 and 64 average monomer repeating units of ε-caprolactone) and different blend compositions (1 wt.%, 2 wt.%, 5 wt.%, 10 wt.% and 20 wt.% of PDLA content) were studied. AFM and TEM analysis revealed a lattice pattern of PLA islands within a PCL matrix, caused by the phase separation of PLA and PCL domains. The average domain spacing d_0 = 12 – 19 nm, determined from SAXS data, was observed to vary with the PDLA and PCL content of the material. A reduction in the PCL average segment length from 64 to 20 repeating units caused the value of d_0 to decrease from 17.7 nm to 15.8 nm. Further, a 5 °C increase in the maximum of the PLA stereocomplex melt transition was observed with a 5 wt.% increase of PDLA content of the matrix, indicating the partial dilution of PCL and PLA amorphous phases within the semicrystalline material. The insight into the phase-separated structure of PCL and PLA containing materials provided here should further facilitate their use in actuator materials whose requirements in terms of thermal and morphological structure closely match those reported here.

Acknowledgments

This work was financially supported by the Helmholtz-Association of German Research Centers (through program-oriented funding, and through the Helmholtz Graduate School of Macromolecular Bioscience [MacroBio], grant no. VH-GS-503). The authors thank Ms. Susanne Schwanz for the XRD and DSC measurements, Ms. Yvonne Pieper for the TEM scans and Dr. Liudmila Lysyakova for the AFM experiments.

References

1. M.A. Hillmyer and W.B. Tolman, *Acc. Chem. Res.* **47**, 2390 (2014).
2. A.-C. Albertsson and I.K. Varma, *Biomacromolecules* **4**, 1466 (2003).
3. S. Farah, D.G. Anderson and R. Langer, *Adv. Drug Del. Rev.* **107**, 367 (2016).
4. T.M. Allen and P.R. Cullis, *Science* **303**, 1818 (2004).
5. P. Saini, M. Arora and M.N.V.R. Kumar, *Adv. Drug Del. Rev.* **107**, 47 (2016).
6. R. Auras, B. Harte and S. Selke, *Macromol. Biosci.* **4**, 835 (2004).
7. M. Hiljanen-Vainio, P. Varpomaa, J. Seppälä and P. Törmälä, *Macromol. Chem. Phys.* **197**, 1503 (1996).
8. H. Liu and J. Zhang, *J. Polym. Sci., Part B: Polym. Phys.* **49**, 1051 (2011).
9. M.J. Fasolka and A.M. Mayes, *Annu. Rev. Mater. Res.* **31**, 323 (2001).
10. J.K. Kim, S.Y. Yang, Y. Lee and Y. Kim, *Progress in Polymer Science (Oxford)* **35**, 1325 (2010).
11. A. Lendlein and O.E.C. Gould, *Nat. Rev. Mater.* **4**, 116 (2019).
12. C. Koning, M. Van Duin, C. Pagnoulle and R. Jerome, *Progress in Polymer Science (Oxford)* **23**, 707 (1998).
13. L. Jiang, M.P. Wolcott and J. Zhang, *Biomacromolecules* **7**, 199 (2006).
14. D. Garlotta, *J. Polym. Environ.* **9**, 63 (2001).
15. M. Labet and W. Thielemans, *Chem. Soc. Rev.* **38**, 3484 (2009).
16. J.-m. Yang, H.-l. Chen, J.-w. You and J.C. Hwang, **29**, 657 (1997).
17. R. Dell'Erba, G. Groeninckx, G. Maglio, M. Malinconico and A. Migliozzi, *Polymer* **42**, 7831 (2001).
18. O.J. Botlhoko, J. Ramontja and S.S. Ray, *Polym. Degrad. Stab.* **154**, 84 (2018).
19. D. Newman, E. Laredo, A. Bello, A. Grillo, J.L. Feijoo and A.J. Muller, *Macromolecules* **42**, 5219 (2009).
20. A.M. Mannion, F.S. Bates and C.W. MacOsko, *Macromolecules* **49**, 4587 (2016).
21. E. Laredo, N. Prutsky, A. Bello, M. Grimau, R.V. Castillo, A.J. Müller and P. Dubois, *European Physical Journal E* **23**, 295 (2007).
22. W. Han, X. Liao, Q. Yang, G. Li, B. He, W. Zhu and Z. Hao, *RSC Advances* **7**, 22515 (2017).
23. D.-d. Yang, W. Liu, H.-m. Zhu, G. Wu, S.-c. Chen, X.-l. Wang and Y.-z. Wang, *ACS Appl. Mater. Interfaces* **10**, 26594 (2018).
24. H. Tsuji, *Adv. Drug Del. Rev.* **107**, 97 (2016).
25. C.L. Wanamaker, W.B. Tolman and M.A. Hillmyer, *Macromolecular Symposia* **283-284**, 130 (2009).
26. Z. Xiong, X. Zhang, R.R. Wang, S. De Vos, R.R. Wang, C.A.P. Joziasse and D. Wang, *Polymer* **76**, 98 (2015).
27. M. Jikei, Y. Takeyama, Y. Yamadoi, N. Shinbo, K. Matsumoto, M. Motokawa, K. Ishibashi and F. Yamamoto, *Polym. J.* **47**, 657 (2015).
28. V. Izraylit, *Private Communication*.
29. G. Perego, T. Vercellio and G. Balbontin, *Die Makromolekulare Chemie* **194**, 2463 (1993).
30. V. Crescenzi, G. Manzini, G. Calzolari and C. Borri, *Eur. Polym. J.* **8**, 449 (1972).
31. H. Tsuji, *Macromol. Biosci.* **5**, 569 (2005).
32. A. Lendlein and S. Kelch, *Angew. Chem. Int. Ed.* **41**, 2034 (2002).
33. S.J. de Jong, W.N.E.E. van Dijk-Wolthuis, J.J. Kettenes-Van Den Bosch, P.J.W.W. Schuyl and W.E. Hennink, *Macromolecules* **31**, 6397 (1998).
34. S. Pensec, M. Leroy, H. Akkouche and N. Spassky, *Polym. Bull.* **45**, 373 (2000).
35. O.V. Stoyanov, R.M. Khuzakhanov, L.F. Stoyanova, V.K. Gerasimov, A.E. Chalykh, A.D. Aliev and M.V. Vokal', *Polymer Science Series D* **4**, 118 (2011).
36. K. Sen, B. Mukherjee, A.S. Bhattacharyya, L.K. Sanghi, K. Bhowmick and R.T. Centre, **157**, 45 (1990).